ION CHANNELS IN SOUTHERN BEAN MOSAIC VIRUS CAPSID

ABELARDO M. SILVA,* RAUL E. CACHAU,‡ AND DANIEL J. GOLDSTEIN§
*Departamento de Fisica, and ‡Instituto de Investigaciones Fisicoquimicas Teoricas y Aplicadas, Facultad de Ciencias Exactas, Universidad Nacional de La Plata, 1900 La Plata, Argentina; and §Departamento de Ciencias Biologicas, Facultad de Ciencias Exactas y Naturales, Universidad de Buenos Aires, 1428 Buenos Aires, Argentina

ABSTRACT The study of southern bean mosaic virus protein coat high resolution model revealed a structure with properties of a natural protein–ion channel. Coat protein pentamers form a 30-Å long channel and the amino acid composition of its wall bears some homology with the pentameric structure proposed for the nicotinic acetylcholine receptor channel. Ion transport properties were analyzed by computing ion–protein interaction energies on the basis of quantum chemistry methods. Energy maps show a channel attractive for cations, fully permeable to Li^+ and a narrow barrier for other cations and water. The energy profiles found are similar to the profiles determined for the K^+ channel of the sarcoplasmic reticulum. Comparisons with other icosahedral virus structures, including picornaviruses, suggest that ion channels would be a common feature of viral capsids. Biological roles for these channels are proposed.

INTRODUCTION

Membrane-bound transport proteins occur in many forms and in all types of biological membranes, but such structures are not yet known at atomic resolution. While studying the structure of southern bean mosaic virus (SBMV), a small icosahedral plant virus, we found that the arrangement and nature of the amino acids immediately around its fivefold axes were such that they might form an ion channel. The molecular structure of the viral capsid is known at 2.8 Å resolution (1, 2), and accurate atomic coordinates are available (3). Thus it was possible to study the properties of the putative channel by computing ion–protein interaction energies.

SBMV has an icosahedral capsid, T = 3, built up by 180 chemically identical subunits (28,214 daltons) (4). The folding motif of the subunit is an eight-stranded antiparallel β barrel. Three quasi-equivalent subunits, differentiated by their symmetry environments, are named A, B, and C. Subunits A are related by icosahedral fivefold axes, creating pentamers. Pairs of subunits B and C related by icosahedral threefold axes create hexamers.

The channel fully spans the protein capsid of the virion and is created by pentamers of subunits A; thus its axis is coincident with icosahedral fivefold axes. Its entrance is at Thr 126 and it extends for 30 Å until Pro 177. There is a wide funnel-shaped structure toward the external viral surface built by a large loop containing Lys 234, the most external residue on the capsid (Fig. 1 *a*). Following the channel, toward the inside of the virion, there is Thr 125, whose methyl groups produce the narrowest section of the channel, and then Trp 162. Three consecutive fivefold rings, each one involving Glu 163, Arg 181, and Asp 178, respectively, end the channel structure (Fig. 1 *b*). Coincidentally, on the basis of sequence data a structure of alternating basic and acidic residue rings has been proposed for the cation channel of the nicotinic acetylcholine receptor, which has a pentameric structure as well (5).

METHODS

Ion–protein interaction energies were computed using a method recently developed by S. Fraga, which is based on a $1/R$ expansion of the interaction potential and is specially suitable for large molecular associations (6). This method has been parameterized on the basis of atomic pair potentials developed by E. Clementi, which were determined after extensive ab-initio self-consistent field (SCF) calculations (7). These SCF procedures, which are based on the principles of quantum mechanics, do not include empirical parameters. Fraga's pair potentials, specially developed for interactions involving amino acids, have been applied to the study of amino acid recognition and amino acid solvation effects (8, 9). These types of potentials were also successfully used for the study of the gramicidin channel, the anphotericin B-cholesterol channel (10; Fraga, S., personal communication), and intermolecular interactions involving molecules other than amino acids (e.g., hydrocarbons, alcohols and phenols, carboxylic acids, amines, etc.).

The interaction energy between the protein subunits (molecule A) and different type of ions (molecule B) is

Correspondence should be addressed to Dr. Silva at his present address: Instituto de Investigaciones Bioquimicas, Gorriti 43, 8000 Bahia Blanca, Argentina.

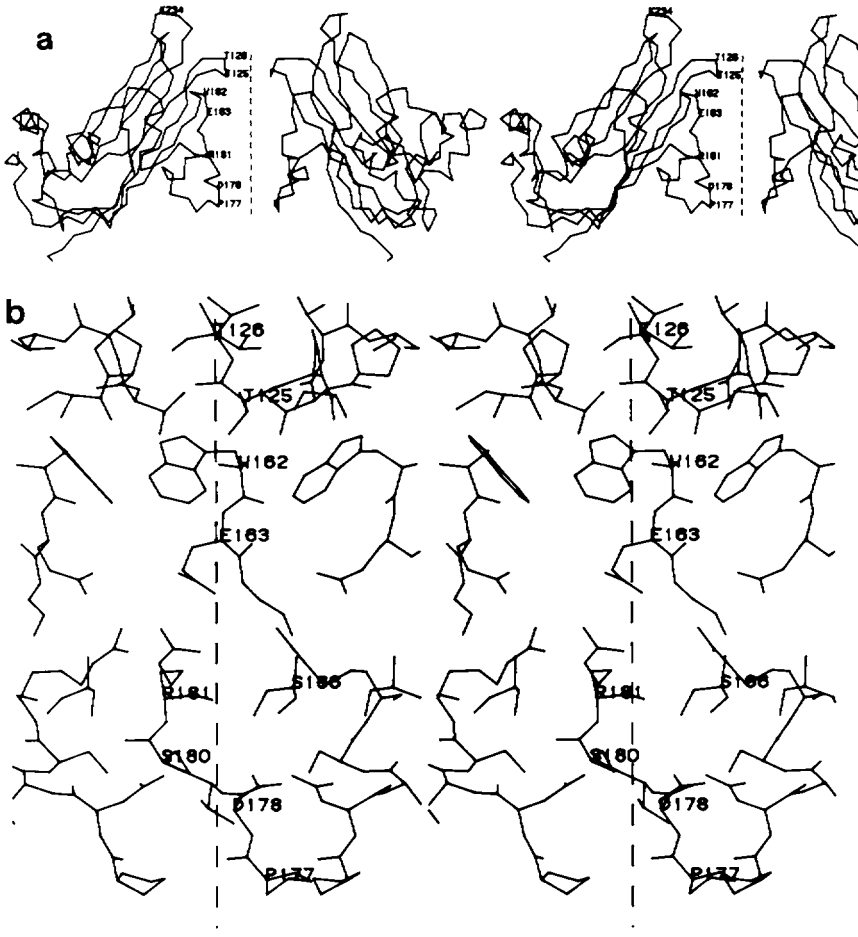

FIGURE 1 (*a*) Stereo view of the C_α backbone of two subunits A around the fivefold axis. The axis of the channel is indicated by a dashed line. The channel (30-Å long) starts at Thr 126 and the main residues lining it have been indicated. A wide funnel is built by the loops containing Lys 234. (*b*) Stereo view of amino acids lining the channel contributed by three out of five subunits. The dashed line is coincident with the line shown in *a*.

expressed as a summation of atomic pair potentials,

$$\Delta E = \Sigma\Sigma\Delta E_{ab}$$

$$\Delta E_{ab} = 1389.4168 Q_a Q_b / R_{ab} - 694.70838(f_a\alpha_a Q_b^2 + f_b\alpha_b Q_a^2)/R_{ab}^4 - 1516.0732 f_a f_b \alpha_a\alpha_b / [(f_a\alpha_a/n_a)^{1/2} + (f_b\alpha_b/n_b)^{1/2}]R_{ab}^6 + 4.184 c_a^{(12)} c_b^{(12)}/R_{ab}^{12},$$

where *a* and *b* indicate atoms of molecule A and molecule B, respectively. The main features of this potential are: (*a*) Its parameters (Q, effective charge; α, dipolar polarizability; f, scale factor; n, effective number of electrons; and c, coefficient for repulsive term) are chosen following the classification proposed by Clementi et al. (11–13). That classification takes into account the nature of each atom as well as its environment in the molecular framework. (*b*) Clementi's pair potentials (11–13) are extracted at the Hartree–Fock (HF) level. Therefore, disregarding fitting deviations on Fraga's potentials, the quality of the results obtained with this potential is that of an HF-SCF supermolecule calculation without electronic correlation; that is, dispersion energies are strongly underestimated. It has to be noticed that for ion–protein interactions underestimation of dispersion terms is less important than a correct evaluation of coulombic and polarization terms. (*c*) The $1/R$ form of the potential allows for analytic gradient optimization of the energy function extremes.

The channel protein structure was considered as rigid, except at the putative gate, for the ion–protein energy calculations. Although dynamic effects in the ion transport phenomenon are recognized as important (14, 15), a static picture provides very valuable information to assess ion conducting properties. Then, either molecular dynamics or energy refinement procedures would be required for a more detailed study of the problem.

Those atoms within a cylinder of 18 Å radius around the axis of the channel (2,250 atoms) were used for the calculations. Thus the isopotential maps reported account for the effect of amino acids located far away from the axis. The maps display similar features if a narrower cylinder, including only 950 atoms, is used. Since the positions of H atoms were not experimentally determined, they were added to the protein structure following geometrical criteria. The location of those H atoms at the channel wall was optimized taking into account interatomic contacts.

Isopotential maps were computed for dehydrated Li^+, Na^+, and K^+ on a plane containing the axis of the channel (Fig. 2 *a*). The plane chosen gives the most asymmetric

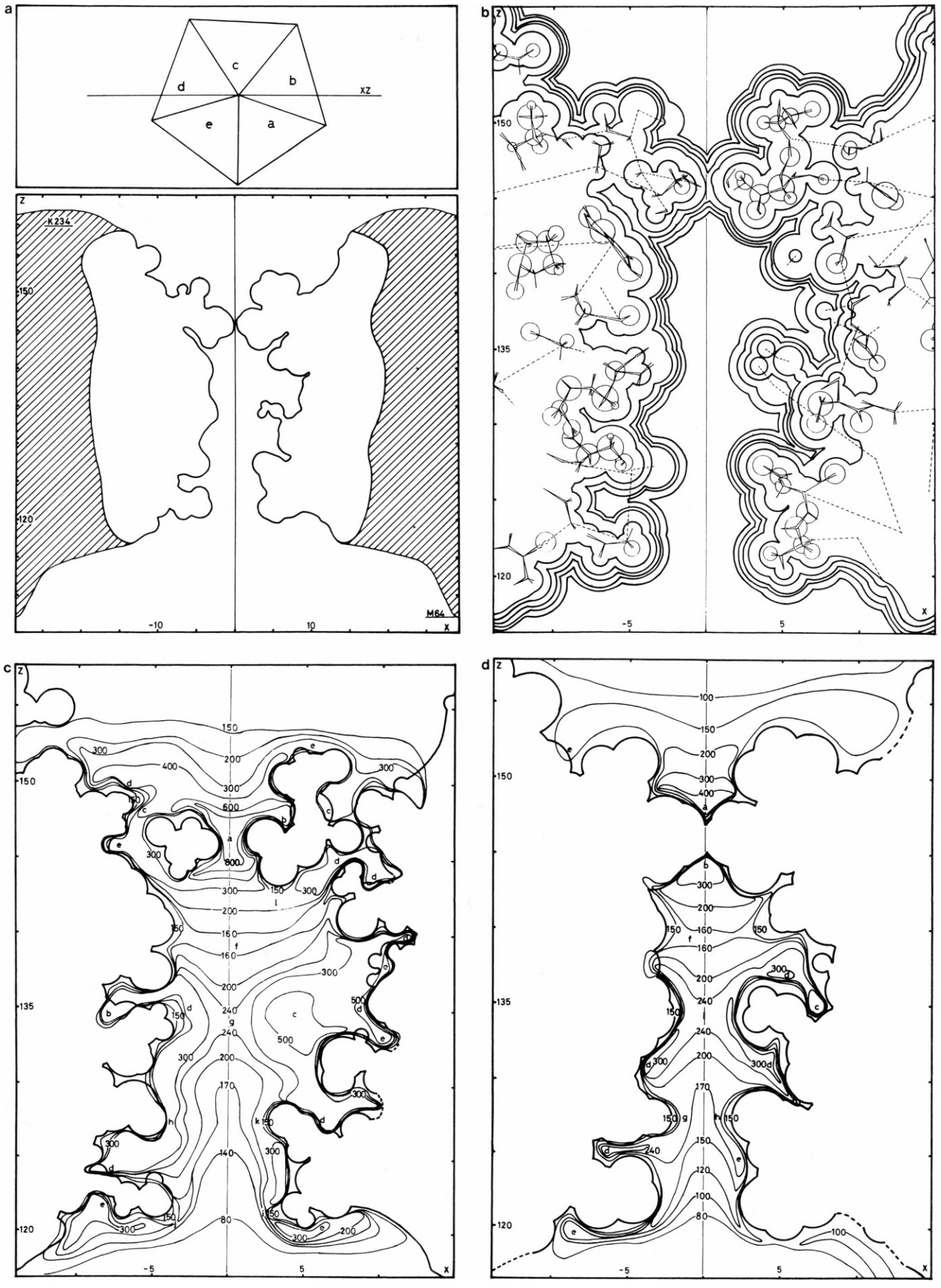

FIGURE 2 (*continued*)

profile for the accessible surface of the channel (Fig. 2 *b*). Due to the fivefold rotational symmetry of the structure, the map on that plane reflects the overall isopotential function. Furthermore, extremes were characterized using a steepest descent technique, which allows searching beyond the plane. Thus the maximum, minimum, and saddle point energies quoted correspond, in general, to values in space. To determine the limits of the isopotential map to be computed, the accessibility surfaces for different ions were calculated (Fig. 2 *b*). They were defined in terms of Van der Waals radii and indicate that the channel is sterically open for Li^+ and Na^+.

RESULTS

As expected the values of the attractive terms of the interaction energies are about one order of magnitude larger than normal since this is an in vacuo calculation. In contrast, the high values for the repulsive term arise from the assumed rigidity of the structure. In any event rather than the energy values what is important is the general behavior of the interaction energy function. The isopotential maps for dehydrated ions (Figs. 2, *c* and *d*, and 3) show a channel that is strongly attractive for cations at its entrance, although cations have to surmount a barrier equal to their dihydration energies. The channel is fully open for Li^+ but there is a sharp energy barrier for both K^+ and Na^+ produced by a single gate, Thr 125. After the barrier there is no other obstacle for cation transport. A cavity was found where two water molecules would favorably interact with the channel wall with energies of the order of 300 and 100 Kcal/mol, respectively. The cavity is located between 134 and 140 Å in Z and it extends to +9 Å in X (Fig. 3); inclusion of water molecules there would increase the symmetry of the channel. No other region was found with similar properties. In fact this was the only region inside the channel where peaks, which could represent water molecules, were seen in the electron density maps. Those peaks were low although clearly above the noise level (3).

The minimum at 125 Å in Z and −8 Å in X would provide an access for highly charged cations towards an extended attractive region defined by sulfurs of the disulfide bridge Cys169-Cys176 and by oxygens from Cys 169, Lys 175, Cys 176, and Thr 179. This corresponds to the location of several heavy atom sites used for the determination of the structure (16).

A minimal energy pathway was computed only for Na^+ (Fig. 3), showing an energy profile analogous to the energy values at the axis (Fig. 4 *a*). Therefore, axial energy profiles properly describe the ion–channel energetic features. From axial energy profiles it is concluded that the channel would be adequate for transport of Ca^{++} and water as well, but there is also a sharp energy barrier at the gate (Fig. 4 *c*). The conductivity for different ions would be mainly determined by this barrier. However, due to the rigidity of the structure unrealistically high repulsive energies are found at the Thr 125 gate for most ions. Peak energy values (Kcal/mol) at Thr 125 are: 700 for Na^+; 1,100 for K^+; 2,000 for Ca^{++}. A more realistic view of the movement of ions in that region requires, at least, some twisting of Thr 125. Thus, the possibility of reducing the energy barrier was analyzed in terms of a synchronous movement of fivefold related Thr 125 towards the inside of the channel (Fig. 1 *b*). The movement was achieved by allowing a full flexibility of the peptide bond of Thr 125. It was quantified by the well known CNDO/2 technique (17), using 98 atoms belonging to Thr 125 and neighboring amino acids from each subunit. The interaction with the rest of the structure was expressed in terms of Fraga's pair potentials as a molecular mechanics. This study shows a very flat energy surface if Thr 125 moves toward the cleft in between fivefold related Trp 162, leading to a considerable reduction of the energy barrier. For Na^+ the movement involves a 8.5° twist, displacing the methyl groups of Thr 125 ~ 1.0 Å from their initial positions and increasing the diameter of the channel 0.6 Å.

The model analyzed has the methyl group of Thr 125 pointing towards the external viral surface. In fact the 2.8 Å resolution electron density maps were slightly ambiguous in that region allowing for two different conformations for Thr 125. These are obtained by a 180° rotation of the side chain around the C_α—C_β bond. In the second case the methyl groups point toward the inside, the distances between them are larger and the hydroxyl groups are external producing the narrowest section of the channel.

FIGURE 2 (*a*) Codification of subunits around the fivefold axis. XZ is the plane chosen for the computation of isopotential maps. In the lower part is shown the intersection of the XZ plane with the accessible surface of the channel defined in terms of Van der Waals radii of protein atoms plus Na^+ radius. The atoms used for the calculations extend up to the shaded region. (*b*) Intersection of the XZ plane with the accessible surface of the channel for different ionic radii. The profiles correspond, from the farthest away from the axis to the nearest one, to Li^+ (Mg^{++}), Na^+ (Ca^{++}, Sr^{++}, H_3O^+), K^+ (Ba^{++}, F^-), NH_4^+ (OH^-), and Cs^+ (Cl^-, Br^-); in parentheses are indicated species of ionic radius similar to the preceding ion. Circles around atoms indicate the intersection of the XZ plane with spheres defined by Van der Waals radii. The amino acids drawn are identified in Fig. 3. The profile for Li^+ is mainly determined by nonhydrogen atoms, whereas on the other extreme the profile for Cs^+ is basically determined by hydrogens. Na^+ is an intermediate case, leading to the most asymmetric profile. (*c*) Isopotential map for Li^+. Energies were computed on a grid of 0.3 by 0.3 Å. In all maps the ion at infinity defines zero energy, quoted energy values are negative, and they are expressed in Kcal/mol. Extremes were characterized by gradient techniques using step of 0.1 Kcal/mol. The minima are (*a*) −1,400; (*b*) −1,100; (*c*) −900; (*d*) −800; (*e*) −500. The saddle points are (*f*) −155; (*g*) −250; (*h*) −320; (*i*) −200; (*j*) −175; (*k*) −250. This is the only case analyzed where a barrier was not found at Thr 125. (*d*) Isopotential map for K^+. Its meaning and computation are as in *c*. The minima are (*a*) −590; (*b*) −490; (*c*) −450; (*d*) −350; (*e*) −200. The saddle points are (*f*) −155; (*g*) −185; (*h*) −180; (*i*) −250. The map shows an energy barrier at Thr 125.

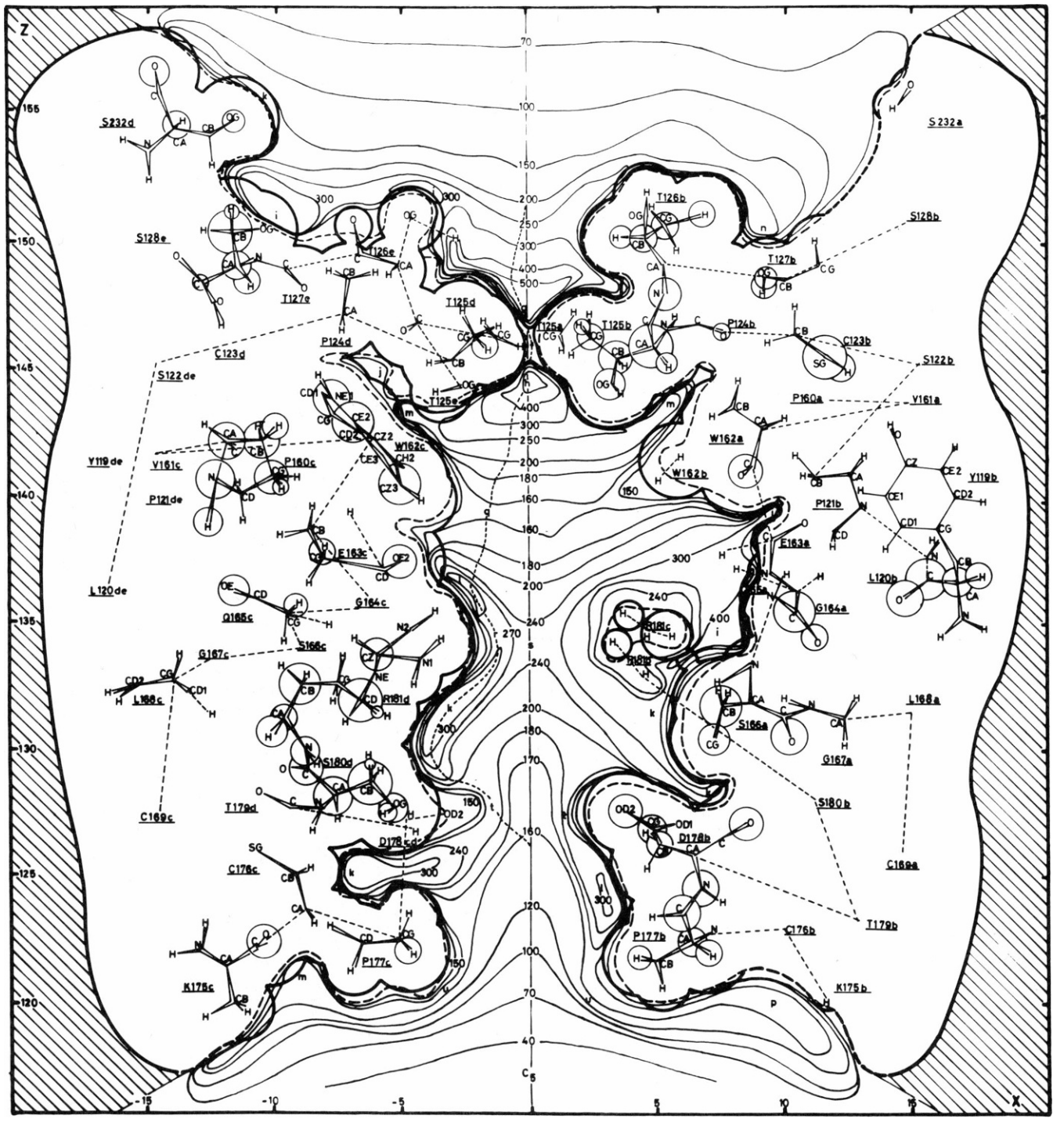

FIGURE 3 Isopotential map for Na^+. The map was computed on a grid of 0.2 by 0.2 Å. The dashed line near by the profile of the accessible surface is the +1,000 Kcal/mol isopotential contour. The maximum value of the map is a saddle point, (*f*) 500; this was determined by gradient techniques, as the other extremes, taking into account the rotation of the methyl group of Thr 125 around the C_γ—C_β bond. The minima are: (*g*) −800; (*h*) −600; (*i*) −500; (*j*) −450; (*k*) −400; (*l*) −350; (*m*) −300; (*n*) −250; (*p*) −200. The saddle points are: (*q*) −155; (*r*) −280; (*s*) −250; (*t*) −190; (*u*) −165. The dashed line by the axis indicates the minimal energy pathway. It was computed by forcing the path to coincide with the axis at the entrance and exit, which is justified since the sections of the channel are quite narrow at those ends. Hydration of viral exposed surfaces would make those sections even narrower. The energy surfaces are quite flat in two regions along the pathway, (136–141 Å) and (122–129 Å) in *Z*.

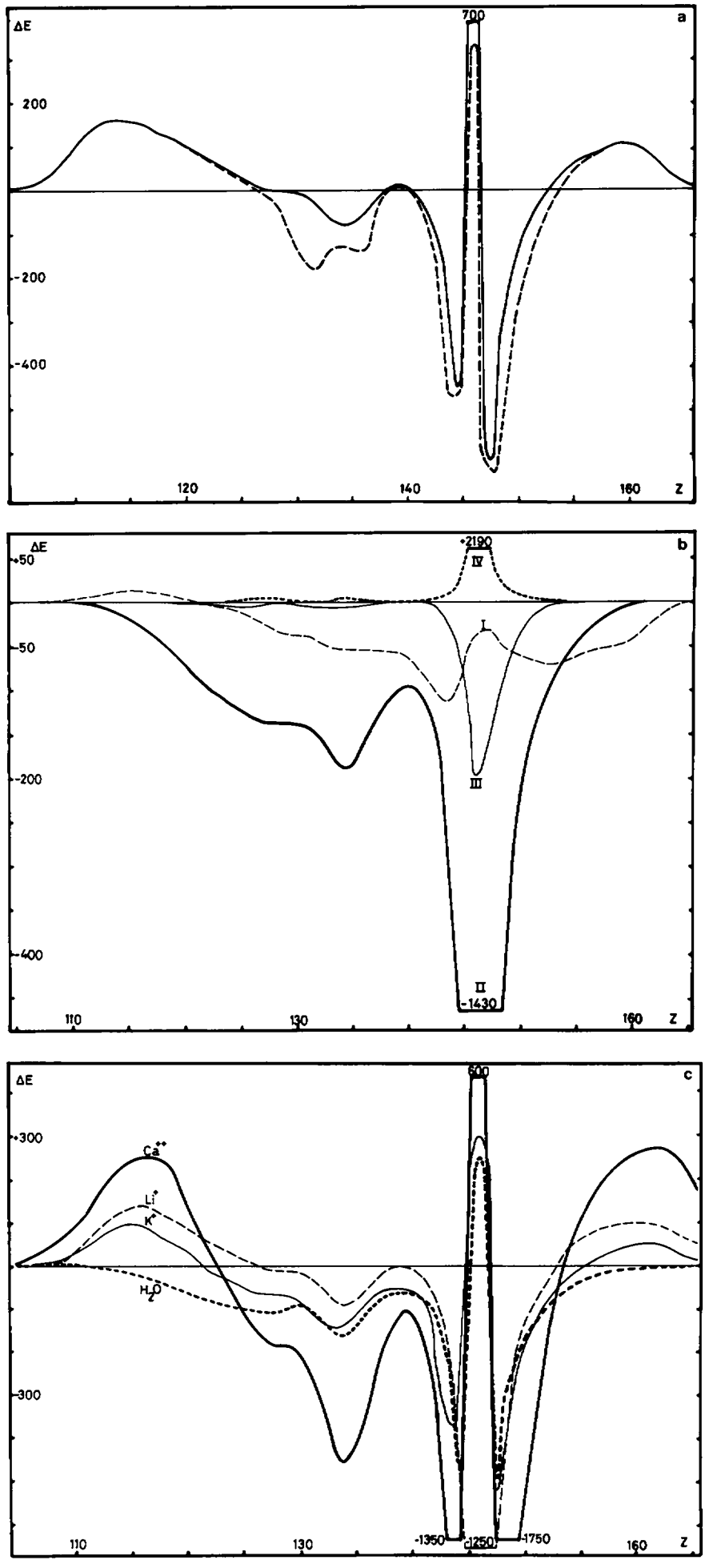

FIGURE 4 Energy profiles (Kcal/mol) along the channel (Å). Zero energy corresponds to the ion in water at infinite dilution, that is, energies differ from the values shown in the maps (Figs. 2 and 3) by a constant equal to the energy required to dehydrate the ion. (*a*) Axial energy profile for Na^+. (*Solid line*) Energy values on the channel axis. Peak value at Thr 125 corresponds to frozen, crystallographically determined, structure. (*Dashed line*) Projection of energy values at the minimal energy pathway (Fig. 3) on the channel axis. Peak energy value corresponds to Thr 125 twisted conformation. Barriers at $z = 150$ Å are reduced to ~ -100 Kcal/mol for the second conformation of Thr 125 after twisting. (*b*) Decomposition of energy terms contributing to the axial energy profile for Na^+. I, coulombic; II, polarization; III, dispersion; IV, repulsive. The large contribution of the polarization term as well as the underestimation of the dispersion is clearly displayed. The ion most affected by errors in the dispersion term is K^+; when corrected the minima are slightly deeper, although the profile has the same features. (*c*) Energy profiles at axial pathways for different ions. Peak energies were computed with Thr 125 twisted conformation. Similar profiles are obtained for NH_4^+ and H_3O^+. Barriers at $z = 150$ Å are reduced to ~ -100 Kcal/mol for the second conformation of Thr 125 after twisting.

This conformation was analyzed as before and it was found that a 6.5° twist of Thr 125 would produce the lowest interaction energy with a virtual disappearance of the energy barrier for the ions studied. In this conformation there is, in fact, a small barrier (−100 Kcal/mol), which arises from a rotation of hydroxyl H induced by steric constraints during Thr 125 twisting. Only NH_4^+ and H_3O^+ display barriers in this configuration, 200 and 300 Kcal/mol high, respectively, although mainly dominated by steric interactions. It should be noticed that the second conformation of Thr 125 is not accessible from the first one, that is, the conformation is defined when the capsid is assembled. In terms of protein–protein interaction energies, this conformation is not as favorable as the original one. In any event both of them are consistent with an ion transport capability for the structure although with different ion selectivity.

Partial hydration of the ions would not change the general features of the potentials since the axial water potential shares common features with the dehydrated ion potentials (Fig. 4 *c*). These results do not suggest any general dehydration mechanism except for Li^+, whose attached water molecules would see a sharp energy barrier at Thr 125 where the cation could pass through. Remarkably, there is a high agreement between the axial potentials found and the potential proposed by Cukierman et al. (18) for the K^+ channel of the sarcoplasmic reticulum, which was based on Cs^+ blocking experiments. They not only display four barriers with a sharp one at the entrance, implying a single gating structure (Thr 125 in our case), but also the relative heights for both K^+ profiles are quite similar.

DISCUSSION

Variations of virion density detected in Cs^+ salt gradients indicate that many icosahedral capsids, including SBMV, would be permeable to Cs^+ (19–21). Our results show a channel sterically closed for Cs^+ (Fig. 2 *b*). Despite the fact that the intricate interlocking of the subunits suggests that no other regions of the capsid would be adequate for ion transport, we could not claim that Cs^+ permeability would be mediated by these channels, although we think it is very likely. The phenomenon is observed at high salt concentrations, therefore large configurational changes are conceivable not only at the channel entrances, thus increasing Cs^+ conductivity, but also at other points on the capsid.

In another two icosahedral plant virus whose structure has been determined, there are Thr residues around the fivefold axis towards the external viral capsid as Thr 126 and Thr 125 in SBMV. In tomato bushy stunt virus (TBSV) (21, 23), Thr 170, Thr 171, and Trp 207 can be structurally superimposed to Thr 125, Thr 126, and Trp 162, respectively, in SBMV (24, 25). That is, the channel entrance structure is similar in both virions even though the homology between amino acid sequences is only 20%. The region between residues 163 and 184 in SBMV, contributing acidic and basic residues to the channel wall, is an insertion relative to TBSV. In satellite tobacco necrosis virus (STNV) (26, 27) a loop containing Thr 138, Gly 139, and Glu 140 approaches the fivefold axis, with Thr 138 being on the external surface. Here Thr and Glu residues are further away from the fivefold axis than in SBMV. This is a short channel locked by a dihydrated ion coordinated to five main chain carbonyl oxygens from Thr 138. Finally, there is a remarkable similarity in protein folding as well as in subunit packing between plant viruses and recently determined picornaviruses: rhinovirus (28) and poliovirus (29). Ion channels could also be present across their protein coats. In fact a channel-like structure locked by an ion has been observed along the fivefold axes of rhinovirus (30).

Although the predicted ion conductivity of this structure has to be experimentally verified, the emerging picture is that ion channels would be a common feature of icosahedral viruses. Several biological roles could be considered for them. They might be just selective leak channels providing cations to ensure electrical neutrality of the RNA and then stability of the inner viral media. Another possibility is that the channels are related to inducing, in vivo, destabilization of the capsid. In particular swelling of the virions appears to be a key step of the viral cycle since swollen particles seem to release their RNA by interaction with ribosomes (31). Alternatively, parts of viral capsids might become incorporated into the cell membrane, changing its permeability towards conditions favoring viral functions.

Dynamic effects in the interaction between biologically relevant ions and the threonines at the gate might lead to reducing the energy barrier in some conditions, thus increasing conductivity. In this case ion transport properties would be determined by nonspecific factors like ion concentrations, temperature, pH, etc. If specificity in conductivity changes is required, ligand molecules might be needed. In that line of reasoning it is tempting to speculate in a gating mechanism involving phosphorylation of the threonines at the entrance of the channel, since threonines are a common occurrence at all three known plant viruses: TBSV, SBMV, and STNV.

Finally, are the structures of viral coat proteins, and therefore viral ion channel, related through divergent evolution to some membrane ion channel proteins? We will have to wait to know the high resolution structure of some membrane ion channel proteins to attempt an answer, which might give us a hint on the origin of viruses themselves.

We are most grateful to Professor Michael G. Rossmann for his support and encouragement during this work. We thank Dr. John W. Erickson for illuminating comments. We also thank Dr. S. Fraga for comments concerning the use of pair potentials and Dr. C. Stauffacher for a critical

reading of this paper. We are grateful to La Plata University (Argentina) for providing computing facilities where all calculations reported were performed.

Abelardo M. Silva acknowledges financial support from Consejo Nacional de Investigacioues Científicas y Técnicas (CONICET), Argentina.

Received for publication 26 November 1986 and in final form 19 May 1987.

REFERENCES

1. Abad-Zapatero, C., S. S. Abdel-Meguid, J. E. Johnson, A. G. W. Leslie, I. Rayment, M. G. Rossmann, D. Suck, and T. Tsukihara. 1980. Structure of southern bean mosaic virus at 2.8A resolution. *Nature (Lond.)*. 286:33–39.
2. Rossmann, M. G., C. Abad-Zapatero, M. A. Hermodson, and J. W. Erickson. 1983. Subunit interactions in southern bean mosaic virus. *J. Mol. Biol.* 166:37–83.
3. Silva, A. M., and M. G. Rossmann. 1985. The refinement of southern bean mosaic virus in reciprocal space. *Acta Crystallogr.* B41:147–157.
4. Hemordson, M., C. Abad-Zapatero, S. S. Abdel-Meguid, S. Pundak, and M. G. Rossmann. 1982. Amino acid sequence of southern bean mosaic virus coat protein and its relation to the three-dimensional structure of the virus. *Virology*. 119:133–149.
5. Young, E. F., E. Ralston, J. Blake, J. Ramachandran, Z. W. Hall, and R. M. Stroud. 1985. Topological mapping of acetylcholine receptor: evidence for a model with five transmembrane segments and a cytoplasmatic COOH-terminal peptide. *Proc. Natl. Acad. Sci. USA*. 82:626–630.
6. Fraga, S. 1982. Molecular associations and reactions. *In* Current Aspects of Quantum Chemistry. Elsevier Publishing Co., Amsterdam.
7. Clementi, E. 1980. Computational Aspects of Large Chemical Systems. Lecture Notes in Chemistry, Vol. 19. Springer Verlag, Berlin.
8. Fraga, S. 1982. Theoretical prediction of protein antigenic determinants from amino acid sequences. *Can. J. Chem.* 60:2606–2615.
9. Fraga, S. 1983. Recognition of amino acids in solution. I. *J. Mol. Struct.* 94:251–258.
10. Fraga, S., and S. H. M. Nilar. 1983. Theoretical simulation of ionic transport through a transmembrane channel. *Can. J. Biochem. Cell Biol.* 61:856–859.
11. Clementi, E., F. Cavallone, and R. Scordamaglia. 1977. Analitical potentials from "ab-initio" computations for the interaction between biomolecules. 1. Water with amino acids. *J. Am. Chem. Soc.* 99:5531–5541.
12. Clementi, E., F. Cavallone, and R. Scordamaglia. 1977. Analitical potentials from "ab-initio" computations for the interaction between biomolecules. 2. Water with the four bases of DNA. *J. Am. Chem. Soc.* 99:5545–5549.
13. Bolis, G., and E. Clementi. 1977. Analitical potentials from "ab-initio" computations for the interaction between biomolecules. 3. Reliability and transferability of the pair potentials. *J. Am. Chem. Soc.* 99:5550–5558.
14. Kim, K. S. 1985. Microscopic effect of an applied voltage on the solvated gramicidin A channel in the presence of Na^+ and K^+ cations. *J. Comp. Chem.* 6:256–263.
15. Kim, K. S., H. L. Nguyan, P. K. Swaminathan, and E. Clementi. 1985. Na^+ and K^+ ion transport through a solvated gramicidin A transmembrane channel: molecular dynamics studies using parallel processors. *J. Phys. Chem.* 89:2870–2876.
16. Abad-Zapatero, C., S. S. Abdel-Meguid, J. E. Johnson, A. G. W. Leslie, I. Rayment, M. G. Rossmann, D. Suck, and T. Tsukihara. 1981. A description of the techniques used in the structure determination of southern bean mosaic virus at 2.8A resolution. *Acta Crystallogr.* B37:2002–2018.
17. Segal, G. A. 1977. Modern Theoretical Chemistry. Semiempirical Methods of Electronic Structure Calculations. Vols. 7 and 8. Plenum Publishing Corp., New York.
18. Cukierman, S., G. Yellen, and C. Miller. 1985. The K^+ channel of sarcoplasmic reticulum. A new look at Cs^+ block. *Biophys. J.* 48:477–484.
19. Rowlands, D. J., D. V. Sangar, and F. Brown. 1971. Bouyant density of picornaviruses in ceasium salts. *J. Gen. Virol.* 13:141–142.
20. Hull, R. 1977. The banding behavior of viruses of the southern bean mosiac virus group in gradients of ceasium sulphate. *Virology*. 79:50–57.
21. Noort, A., C. L. A. M. Van Den Dries, C. W. A. Pleij, E. M. J. Jaspars, and L. Bosch. 1982. Properties of turnip yellow mosiac virus in caesium chloride solutions: the formation of high density components. *Virology*. 120:412–421.
22. Harrison, S. C., A. J. Olson, C. E. Schutt, F. K. Winkler, and G. Bricogne. 1978. Tomato bushy stunt virus at 2.8A resolution. *Nature (Lond.)*. 276:368–373.
23. Olson, A. J., G. Bricogne, and S. C. Harrison. 1983. Structure of tomato bushy stunt virus IV. The virus particle at 2.9A resolution. *J. Mol. Biol.* 171:61–93.
24. Rossmann, M. G., C. Abad-Zapatero, M. R. N. Murthy, L. Liljas, T. A. Jones, and B. Strandberg. 1983. Structural comparisons of some small spherical viruses. *J. Mol. Biol.* 165:711–736.
25. Hopper, P., S. C. Harrison, and R. T. Sauer. 1984. Structure of tomato bushy stunt virus V. Coat protein sequence determination and its structural implications. *J. Mol. Biol.* 177:701–713.
26. Liljas, L., T. Unge, T. A. Jones, K. Fridborg, S. Lovgren, U. Skoglund, and B. Strandberg. 1982. Structure of satellite tobacco necrosis virus at 3.0A resolution. *J. Mol. Biol.* 159:93–108.
27. Jones, T. A., and L. Liljas. 1984. Structure of satellite tobacco necrosis virus after crystallographic refinement at 2.5A resolution. *J. Mol. Biol.* 177:735–767.
28. Rossmann, M. G., E. Arnold, J. W. Erickson, E. A. Frankenberger, J. P. Griffith, H. J. Hecht, J. E. Johnson, G. Kamer, M. Luo, A. G. Mosser, R. R. Rueckert, B. Sherry, and G. Vriend. 1985. The structure of a human common cold virus (Rhinovirus 14) and its functional relations to other picornaviruses. *Nature (Lond.)*. 317:145–153.
29. Hogle, J. M., M. Chow, and D. J. Filman. 1985. Three-dimensional structure of poliovirus at 2.8A resolution. *Science (Wash. DC)*. 229:1358–1365.
30. Smith, T. J., M. J. Kremer, M. Luo, G. Vriend, E. Arnold, G. Kamer, M. G. Rossmann, M. A. McKinlay, G. D. Diana, and M. J. Otto. 1986. The site of attachment in human rhinovirus 14 for antiviral agents that inhibit uncoating. *Science (Wash. DC)*. 233:1286–1293.
31. Brisco, M. J., R. Hull, and T. M. A. Wilson. 1985. Southern bean mosaic virus-specific proteins are synthesized in an in vitro system supplemented with intact, treated virions. *Virology*. 143:392–398.